ERS – ASAR INTEGRATION IN THE INTERFEROMETRIC POINT TARGET ANALYSIS

U. Wegmüller, C. Werner , T. Strozzi, and A. Wiesmann

Gamma Remote Sensing AG, Worbstrasse 225, CH-3073 Gümligen, Switzerland, http://www.gamma-rs.ch, wegmuller@gamma-rs.ch

ABSTRACT

The possibility to continue deformation monitoring between the rich archive of SAR data acquired by the ERS satellites and ENVISAT ASAR is essential for related applications and services. In many cases the current time monitoring is in the center of the interest, but the existence of the ERS archive is relevant as a record of the deformation history. Another important factor is that the reliability and accuracy of current time monitoring with ASAR is improved by the availability of the historic ERS observations, this particularly in cases where only few ASAR images were acquired.

In this contribution, an approach for the integration of ERS and ASAR data in the Interferometric Point Target Analysis (IPTA) is presented. An important advantage of the use of targets with point like scatter characteristics in a SAR interferometric analysis is that coherence is maintained for many scatterers across series including both ERS and ENVISAT data – this in spite of the slightly different sensor carrier frequencies. The main steps of the integration are the transformation of the ASAR scenes to the ERS reference geometry, the consideration of the different carrier frequencies in the phase interpretation, and the estimation of a point-wise ERS – ASAR phase offset. Based on examples mainly from the mining subsidence application the steps done and the results achieved are discussed.

1. INTRODUCTION

There is a high interest in the use of series of repeat-track SAR acquisitions for the monitoring of land surface deformation movements. One important advantage of the satellite-based technique is the availability of archived data. The ERS-1/2 archive, for example, contains > 50 repeat acquisitions between 1992 and 2005 for most of Europe as well as for many other parts of the world. While archived data are excellent for the assessment of deformation histories current time monitoring depends on new acquisitions. Given the pointing difficulties of the ERS-2 (gyroscope failures) mainly ENVISAT ASAR and Radarsat-1 are currently used for this purpose. ENVISAT is operated in the same tracks as the ERS satellites, nevertheless at a slightly different carrier frequency, which has a strong influence on across-sensor interferometry.

In this contribution, an approach for the integration of ERS and ASAR data into the Interferometric Point Target Analysis (IPTA) processing is presented. An important advantage of the use of targets with point like scatter characteristics in a SAR interferometric analysis is that coherence is maintained for many scatterers across series including both ERS and ENVISAT data – this in spite of the slightly different sensor carrier frequencies.

An integration of ERS – ASAR series is very relevant for current time monitoring. Furthermore, the accuracy of current time monitoring based on a smaller number of ASAR acquisitions can be improved through the integration of additional ERS acquisitions, e.g. through a better identification of adequate points and through a more accurate estimation of the related point heights.

2. INTERFEROMETRIC POINT TARGET ANALYSIS (IPTA)

Interferometric Point Target Analysis (IPTA) is a method to exploit the temporal and spatial characteristics of interferometric signatures collected from point targets to accurately map surface deformation histories, terrain heights, and relative atmospheric path delays. The use of targets with point like scatter characteristics has the advantage that there is much less geometric decorrelation. This permits phase interpretation even for large baselines above the critical one. Consequently, more image pairs may be included in the analysis. Important advantages are the potential to find scatterers in low-coherence areas and that interferometric image pairs with large baselines may be included in the

analysis. Finding usable points in low-coherence regions fills spatial gaps in the deformation maps while the ability to use large baselines improves the temporal sampling. For a more detailed discussion of the point target based interferometric technique used see [1].

3. ERS – ASAR INTEGRATION

3.1. Sensor characteristics

ERS and ENVISAT ASAR IS2 Mode sensor characteristics are listed in Table 1. The main difference is the different carrier frequency. The differences in the range and azimuth pixel spacing must also be considered in the co-registration of ERS and ASAR SLC.

Table 1 ERS and ENVISAT ASAR IS2 Mode characteristics. Main differences are highlighted in red.

Parameter	ERS	ASAR IS2 VV
SAR_center_frequency	5.300 GHz	5.331 GHz
Polarization	VV	VV
nominal_antenna_look_angle	20.350 deg.	20.138 deg.
Orbits	35-day repeat cycles	Same as ERS, ~30' behind ERS-2
pulse_repetition_frequency	1679.9 Hz	1652.42 Hz
azimuth_pixel_spacing	3.97 m	4.04 m
Doppler spectra	nominal Doppler spectra overlap strongly	
chirp_bandwidth	1.555e+07 Hz	1.600e+07 Hz
ADC_sampling_frequency	1.896e+07 Hz	1.921e+07 Hz
range_pixel_spacing	7.90 m	7.80 m

3.2. Interferogram range phase slope

The range phase is proportional to the slant range distance and the carrier frequency. Interferograms between ERS and ASAR IS2 VV scenes include a range phase ramp related to the different carrier frequencies:

$$\frac{d\phi}{dr} = \frac{4\pi(f_{ASAR} - f_{ERS})}{c} = 1.3 \frac{rad}{m} \quad (1)$$

where ϕ is the interferometric phase, r the slant range, f_{ASAR} and f_{ERS} the ASAR and ERS carrier frequencies, and c the velocity of light. Given a slant range sampling around 8m this means that this phase ramp varies between adjacent slant range pixels by ~10.2 radian, this is more than a full phase cycle.

This range phase trend needs to be taken into account in across sensor interferograms. Typically, this is done by including this trend in the simulated phase used to calculate the differential interferogram. Furthermore, an "effective frequency" corresponding to the average of the two carrier frequencies is used in the calculation of the topographic and deformation phase terms.

3.3. Across sensor differential interferograms

Apart from the above-mentioned effects of the different carrier frequencies coherence considerations are necessary. The range spectra of ERS and ASAR do not overlap, i.e. the offset between the carrier frequencies (31 MHz) is significantly larger than the range spectra width (around 16 MHz). For distributed targets and short baselines we expect therefore very low correlation of the signals. Under special conditions it is possible though, that the observed reflectivity spectra of distributed targets do overlap so that coherence can be observed in spite of the different carrier frequencies. This is

the case if the view angle or baseline effect on the reflectivity spectra approximately compensates the carrier frequency difference. For ERS and ASAR IS2 this is possible with baselines $B_\perp$ between about 1.4km and 2.4 km, with the lower frequency sensor (ERS) having the slightly higher incidence angle (i.e. the ERS sensor needs to be further East than the ASAR sensor for descending orbits and further West for ascending orbits).

Confirmation is obtained from the ERS2-ASAR IS2 VV differential interferogram over the larger Paris area, shown in Figure 1. Both the ERS and ASAR scenes were acquired on 7-Dec-2002 within about 28 minutes (ASAR at 11:14, ERS2 at 11:42). The perpendicular baseline B⊥ varies between 1562m at near range and 1494m at far range. The azimuth spectra overlap is only about 500 Hz (ERS2 was in Zero-Gyro mode). Spatially adaptive azimuth and range common band filtering was applied, considering the baseline and frequency offset effects. The common range bandwidth varies between 0.64 at near range and 0.16 at far range. The above discussed range phase trend was considered and the average of the two carrier frequencies was used in the simulation of the topographic phase, using the SRTM 3" DEM.

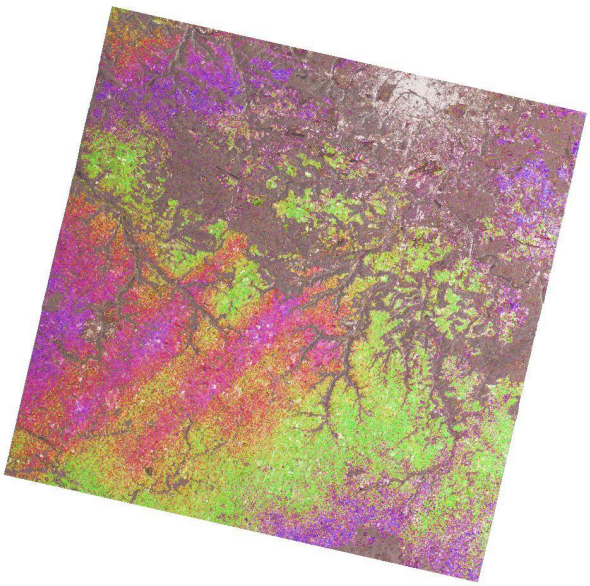


Figure 1 ERS2 – ASAR IS2 VV "30-minutes" differential interferogram. One color cycle corresponds to one 2π phase cycle. ERS and ENVISAT raw data courtesy CAT1_2452 (PI Wegmüller).

In the ERS2 – ASAR IS2 VV "30-minutes" differential interferogram high coherence (low phase noise) is observed for the majority of the agricultural fields to the south of Paris. At this time of the year (7. Dec.) most fields are bare or only sparsely covered with vegetation. Low coherence is observed for forest and for the city area with geometric decorrelation related to the large baseline being the likely explanation.

The phase observed is most likely related to path delay heterogeneities in the troposphere. This is an impressive confirmation that the atmospheric path delay pattern can significantly change within 30 minutes!

3.4. Across sensor differential interferograms for point targets

In the previous section distributed targets and "conventional interferometry" were considered. For point targets the scattering is uniform into all directions; there is no view angle or baseline effect comparable to the "spectral shift" of distributed scatterers. But, In the case of a resolution cell with a dominant point target the "ERS2-ASAR phase ramp correction" needs to be applied not for the pixel center but for the actual location of the point target scattering phase center. Relative to the pixel center this means a difference in this correction between ± 5.1 radian (which is more than a full phase cycle).

For an IPTA analysis this means that for each pixel such an ERS - ASAR phase offset ϕ_{EA} needs to be considered. For every pixel the sub-pixel location of the phase center of the dominant point scatterer is different, consequently, ϕ_{EA} differs from point to point (looking like noise); but for a selected point the same offset ϕ_{EA} applies for all ERS – ASAR pairs.

Confirmation of this behavior is sought in a small IPTA experiment. The data used include a large ERS data stack and several ASAR IS2 VV acquisitions, all acquired in the same track over the same area. An interferometric point target analysis has already been conducted on the ERS scenes, resulting in a list of point coordinates, and related point heights, deformation values, atmospheric phase corrections, and quality information.

As a first step the ASAR SLC are co-registered to the ERS reference SLC. Then, for the points accepted in the ERS IPTA, and using the ERS IPTA derived point heights and point linear deformation rates point differential interferograms are calculated. For ERS – ASAR pairs the ERS-ASAR phase ramp (see discussion under 3.2.) calculated for the pixel centers was included in the simulated interferometric phases. For the ERS scenes the atmospheric phase corrections were subtracted from the differential interferograms. In addition to the ERS – ERS pairs ASAR – ASAR pairs and ERS – ASAR pairs were included in the data stack.

For ASAR – ASAR pairs we found that the resulting point wise differential interferometric phases look spatially "smooth", and this even for large baselines as shown in Figure 3 for a pair with a perpendicular baseline of more than 800m. This means that the points selected based on the ERS data stack (i.e. points with a temporally coherent point like scattering behavior) are also a useful selection for the ASAR scenes. Furthermore, the point heights determined from the ERS data stack can directly be used for the ASAR data. The same points and point heights can be used. The most likely interpretation is, of course, that the same scatterers are dominant in the ERS and in the ASAR data, in spite of the slightly different carrier frequency.

For ERS – ASAR pairs we observe that the resulting point wise differential interferometric phases look spatially "noisy", as shown in Figure 2. This is not surprising, as these phase still include the point-wise ERS - ASAR phase offset related to the sub-pixel position of the phase center, which can vary between –5.1 radian and +5.1 radian. For a selected point this phase offset f_{EA} is expected to be the same for each ERS – ASAR pair. Consequently, we can consider one of these ERS – ASAR pairs (e.g. pairs E47 – A65) as a simple estimation of this phase offset f_{EA} (unwrapping is not necessary here) and subtract it from the other ERS – ASAR point differential interferograms. We find that all these phase offset corrected ERS – ASAR point differential interferograms look spatially smooth, as shown in Figure 4 this is the case even for pairs with large baselines.

This finding shows that an initial ERS – ASAR phase offsets estimate is easily obtained from a single ERS – ASAR pair. To evaluate the limitations of this simple approach we consider the phase of the differential interferogram used to estimate the phase offset f_{EA}

$$\phi = \phi_{EA} + \phi_{atm} + \phi_{ddef} + \phi_{dhgt} + \phi_{dbase} + \phi_{noise} \quad (2)$$

The differential interferometric phase is a sum of ϕ_{EA} the phase offset, ϕ_{atm} an atmospheric phase term which includes the atmospheric phase correction for the ASAR acquisition (as well as the errors of the atmospheric phase correction estimated for the ERS acquisition), ϕ_{ddef} the deformation model phase error, ϕ_{dhgt} the height model phase error, and ϕ_{noise} phase noise. The main error term in the ϕ_{EA} estimation is the atmospheric phase term. This error can be minimized by selecting an ASAR acquisition with low atmospheric distortions (as found for example from considering ASAR – ASAR differential interferograms.

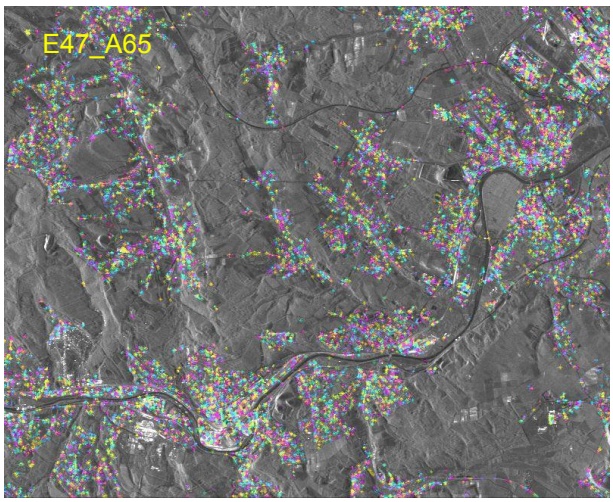
3.5. ERS – ASAR phase offsets estimation from multiple ERS – ASAR pairs

The point-wise ERS – ASAR phase offsets can be estimated as part of the regression analysis. In addition to the phase model which describes the time and baseline dependence a pixel-wise ERS – ASAR phase offset is considered. In the case of a linear deformation model this corresponds to searching two parallel planes (defined by the two y-axis offsets and two slopes) which deviate minimally from the ERS – ERS (first plane) and ERS – ASAR (second plane) differential phases.

The simplistic (but very straight forward) method presented in Section 3.4 sacrifices one ASAR observation; for the observation used to determine the point-wise ERS – ASAR phase offsets the value will correspond exactly to the model value. Determining the point-wise ERS – ASAR phase offsets in a regression analysis does not have this disadvantage.

4. RESULTS

An example of a result is shown in Figure 5. The area considered includes stable as well as subsiding and slightly uplifting areas. The last 10 values of the time series shown correspond to the ASAR observation, the earlier values to the ERS observations. The integration of the ERS and ASAR observations was successful.



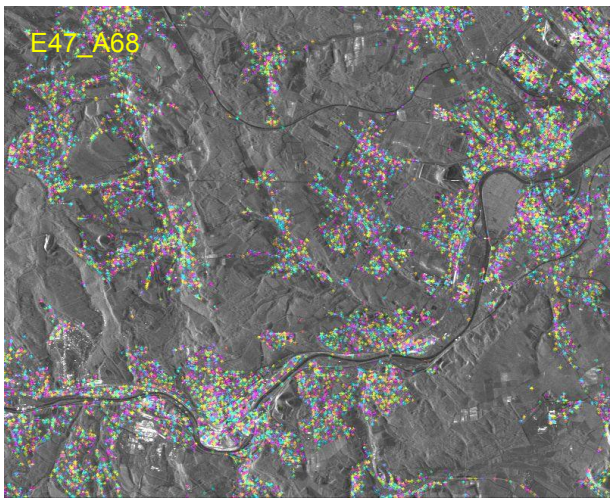


Figure 2 ERS – ASAR point differential interferograms (without consideration of sub-pixel range position of dominant scattering phase center). One color cycle corresponds to one 2π phase cycle. ERS and ENVISAT raw data ©ESA.

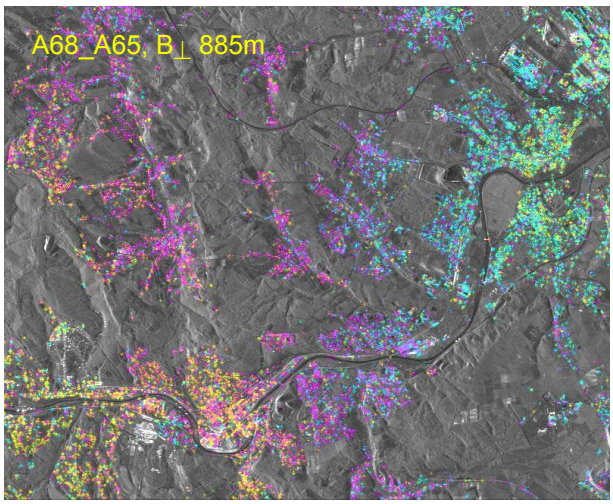


Figure 3 ASAR – ASAR point differential interferogram. One color cycle corresponds to one 2π phase cycle. ERS and ENVISAT raw data ©ESA.

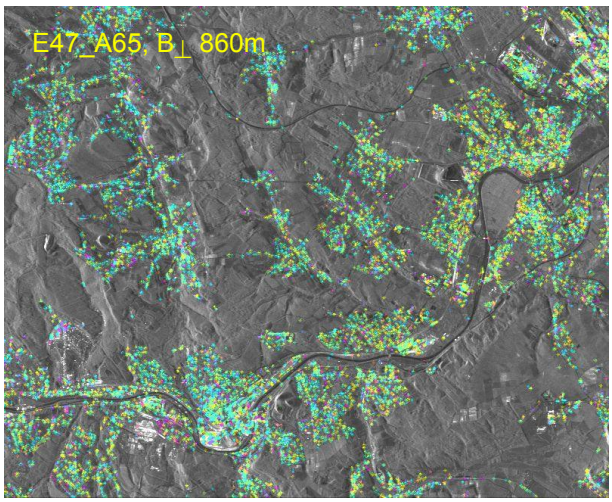


Figure 4 ERS – ASAR point differential interferogram (after subtraction of sub-pixel range position of dominant scattering phase center estimated from ERS – ASAR pair E47_E68). One color cycle corresponds to one 2π phase cycle. ERS and ENVISAT raw data ©ESA.

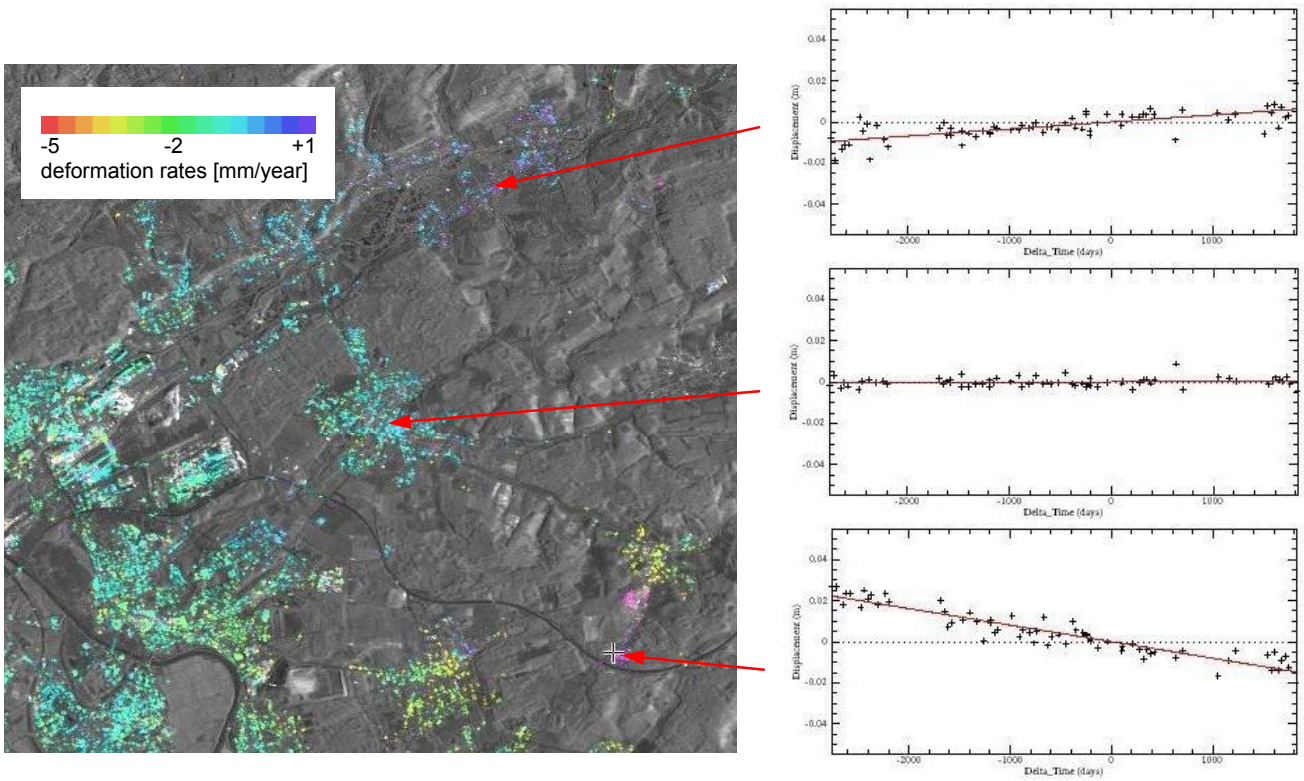


Figure 5 LOS displacement rates (left side) and selected deformation histories derived from an ERS and ASAR data stack. Negative values correspond to subsidence. ERS and ENVISAT raw data ©ESA.

5. CONCLUSIONS

A simple method to integrate ERS and ASAR data into a single IPTA time series was presented. The ERS and ASAR observations are *fully integrated* in the sense that the same scatterers are considered, the same point heights are used and ERS – ASAR pairs are directly included in the same way as ERS – ERS pairs except for the additional ERS – ASAR phase offset which is considered for ERS – ASAR pairs. This phase offset is related to the sub-pixel range position of the phase center of the dominant scatterer, varies between –5.1 radian and +5.1 radian and looks spatially random. An initial estimate of the ERS - ASAR phase offsets is the phase of an ERS – ASAR point differential interferogram; preferably using an ASAR acquisition with low atmospheric distortions. This simplistic estimate of the ERS - ASAR phase offset is sufficient to get spatially smooth, interpretable, ERS – ASAR point differential interferograms. An ERS - ASAR phase offset estimate based on all the available data is obtained by including the ERS - ASAR phase offset in the two-dimensional regression analysis.

The demonstrated feasibility of the integration of ERS and ASAR data into single IPTA time series and the relative simplicity of the approach used are extremely positive for current time land motion monitoring using ASAR data. It is very likely that the same kind of integration will also be possible between Radarsat 1 and Radarsat 2. A detailed analysis of the *quality* of the ERS based point selection and point heights was not possible with only 10 ASAR scenes complementing the large ERS data stack. Evaluating temporal series and spatial coherence indicates that almost all (>90%) of the points identified using ERS can still be used for the ASAR observations.

6. REFERENCES

[1] Wegmüller U., C. Werner, T. Strozzi, and A. Wiesmann, “Multi-temporal interferometric point target analysis”, in Analysis of Multi-temporal remote sensing images, Smits and Bruzzone (ed.), Series in Remote Sensing, Vol. 3, World Scientific (ISBN 981-238-915-61), pp. 136-144, 2004.